scientific reports

OPEN

Research on parameter optimization design of coreless transformer based on genetic algorithm

Wenshuang Qin[1], Yi Zhang[1] & Yufang Lu[2]✉

This study found that the inter-coil spacing (H) of a coreless transformer, the operating frequency (f_0), the load (R_L) on the transformer's secondary circuit, and the actual operating frequency (f) all affect the transmission efficiency (η) of the transformer. To address this, a random forest regression model was used to predict the transmission efficiency (η) as a function of the parameters (f_0, H, R_L, f). A genetic algorithm was employed to optimize the parameters (f_0, H, R_L, f) in order to maximize η. Based on the optimization results, efficient transformer and circuit designs were developed. After simulation verification, a prototype circuit was fabricated and tested. The results showed that the transmission efficiency of the planar coreless transformer, optimized using the genetic algorithm, reached 71.7%, a 54.8% improvement over the unoptimized circuit and a 17.7% increase compared to the directly designed transformer circuit without optimization. This demonstrates the effectiveness of the proposed optimization approach.

Keywords Planar coreless transformer, Genetic algorithm, Parameter optimization, Transmission efficiency

In high-density circuit design applications, such as those in the aerospace sector, there are stringent requirements on circuit miniaturization and performance. Employing low-profile magnetic components arranged in planar or pancake-type configurations can significantly reduce the overall device size[1], thereby facilitating system weight reduction. In the field of magnetically or near-field coupled Wireless Power Transmission (WPT), extensive research has been conducted on planar coil design[2–4]. Our previous research investigated the influence of coil design parameters, including trace width, spacing, and the number of turns (N), on key performance metrics such as self-inductance (L), quality factor (Q), coupling coefficient (k), and power transfer efficiency[5]. Building on these findings and further analysis based on wireless power transfer theory, it becomes evident that the maximum transmission efficiency of the transformer circuit may not reach its theoretical limit if the design process fails to comprehensively account for the effects of coil coupling strength, impedance matching, and coil losses. Relying solely on a single-stage impedance matching approach may hinder the circuit from achieving optimal transmission efficiency, thereby falling short of the maximum efficiency attainable with the designed transformer configuration. Consequently, such circuits exhibit low power transfer efficiency, particularly in gate driver applications. After rectification and filtering, the signal received by the transformer secondary is typically fed into a push–pull circuit. The resulting low transmission efficiency reduces the secondary circuit's load-driving capability, which may lead to functional instability or circuit failure. Therefore, this paper proposes an algorithmic optimization framework that jointly optimizes four key parameters—f_0, H, R_L, and f—to accelerate circuit design toward achieving the maximum transmission efficiency attainable with the designed transformer configuration. The proposed approach streamlines the design process by reducing complexity while maintaining high transmission efficiency.

In this paper, a coil model is established in Ansys Maxwell, considering the coil area constraints in practical circuit applications, with design parameters including line width, line spacing, line thickness, and the number of turns. The coil model is co-simulated with the external circuit in Ansys Simplorer. The simulation results indicate that the energy transmission efficiency varies with different combinations of parameters (f_0, H, R_L, f). Therefore, under a specific set of coil design parameters, an initial population is generated by defining different combinations of these four parameters. The corresponding transmission efficiency data are obtained through co-

[1]School of Computer Science and Engineering, Guilin University of Technology, Guilin 541004, Guangxi, China. [2]School of Information and Communication, Guilin University of Electronic Technology, Guilin 541004, Guangxi, China. ✉email: luyufang@guet.edu.cn

simulation. Based on genetic algorithm (GA) principles, the fitness of each parameter combination is evaluated in MATLAB. The optimal combination is then determined via selection, crossover, and mutation operations, corresponding to the highest achievable transmission efficiency. Thus, the data analysis and optimization process is accomplished. The optimization results enable more efficient design of circuits with higher transmission efficiency. This approach has been validated through simulation, and both the prototype circuit design process and experimental results further verify the feasibility of the proposed method. For ease of reference, a glossary of symbols is provided at the end of this paper.

Coupling analysis of planar coreless coil

The coupling coefficient k between the planar primary and secondary coils can be expressed in terms of the mutual magnetic flux Φ linking the coils.

$$k = \frac{\Phi_{21}}{\Phi_1} = \frac{\Phi_{12}}{\Phi_2} \tag{1}$$

$$\Phi = \int \mathbf{B} \cdot d\mathbf{A} \tag{2}$$

In the equation, $\mathbf{B}$ denotes the magnetic flux density, and $\mathbf{A}$ represents the infinitesimal area element of the coil. Φ_{21} and Φ_{12} denote the magnetic flux in coil 2 induced by the current I_1 in coil 1, and the flux in coil 1 induced by the current I_2 in coil 2, respectively. Φ_1 and Φ_2 represent the total magnetic flux linking coils 1 and 2, respectively. According to Faraday's law of electromagnetic induction and the definitions of self-inductance L and mutual inductance M, the following relations can be derived:

$$
\begin{aligned}
k^2 &= \frac{\Phi_{21}\Phi_{12}}{\Phi_1\Phi_2} \\
&= \left(\frac{N_2\Phi_{21}}{I_1} \cdot \frac{I_1}{N_1\Phi_1} \right) \cdot \left(\frac{N_1\Phi_{12}}{I_2} \cdot \frac{I_2}{N_2\Phi_2} \right) \\
&= \left(M \cdot \frac{1}{L_1} \right) \cdot \left(M \cdot \frac{1}{L_2} \right)
\end{aligned}
\tag{3}
$$

The expression for the coupling coefficient k in terms of self-inductance L and mutual inductance M is derived as follows:

$$k = \frac{M}{\sqrt{L_1 L_2}} \tag{4}$$

Furthermore, in terms of the coil's physical parameters, the self-inductance L of the planar coil is equivalent to the sum of the self-inductance L_i of each individual turn and the mutual inductance M_{ij} between any two turns. This can be mathematically expressed as:

$$L = \sum_{i=1}^{N} \left(L_i + \sum_{j=i+1}^{N} M_{ij} \right) \tag{5}$$

$$L_i = \frac{\mu_0}{8} \left(\ln \frac{8r_i}{d} - 1.75 \right) \tag{6}$$

$$M_{ij} = \frac{\mu_0}{4\pi} \cdot \frac{2\pi r_i r_j}{D_{ij}} \left(\ln \frac{4D_{ij}}{d} - 1 \right) \tag{7}$$

Here, μ_0 is the permeability of free space ($\approx 4\pi \times 10^{-7}$ H/m), r_i and r_j are the radii of the i-th and j-th coil turns, d is the wire diameter, and D_{ij} denotes the distance between the i-th and j-th turns. Theoretically, from Eqs. (5) and (6), it follows that the self-inductance of the coil is governed by the coil design parameters, and once the coil is constructed, its self-inductance becomes fixed. However, in practical high- and medium-frequency operating environments, the skin and proximity effects of the coil conductor become significant. In such cases, the increased parasitic capacitance of the coil counteracts the inductive reactance, resulting in a change in the coil's self-inductance. Figure 1 shows the variation in the primary coil's self-inductance L_T and the coupling coefficient k as the operating frequency increases, obtained from the eddy current field simulation in Maxwell using the parameters in Table 1.

As the operating frequency increases, both self-inductance L_T and the coupling coefficient k of the coil decline. This highlights the limitations of using only parameters such as line width W, line spacing S, and number of turns N to determine self-inductance. In the simulation, when coil spacing H is fixed, varying H while keeping W, S, and N constant leads to significant changes in k, as shown in Fig. 2.

When the coil's W, S, N and wire thickness L_Z are held constant, a smaller H increases the mutual inductance M, which in turn affects the self-inductance L. This results in tighter magnetic flux coupling and an increase in k. Although this is a complex process involving interacting variables, it can be simplified as a variation in coupling transmission efficiency due to changes in H, thus enabling H to directly characterize the coupling efficiency.
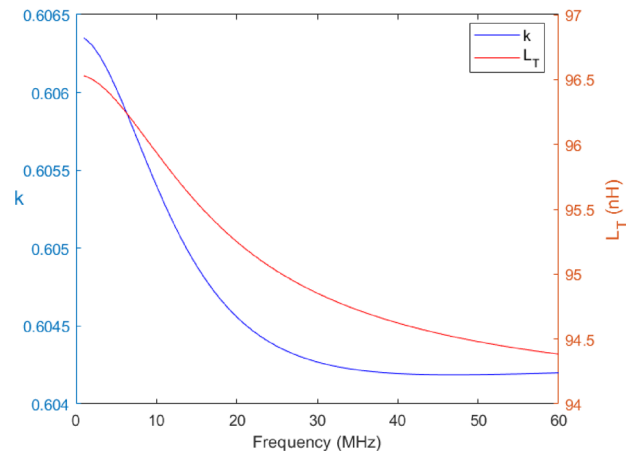
Fig. 1. The coupling coefficient k and self-inductance L_T as a function of frequency.

Parameter	$N_1{:}N_2$	W (mm)	S (mm)	H (mm)	L_Z (mm)
Values	6:11	0.1	0.1	0.1088	0.0152

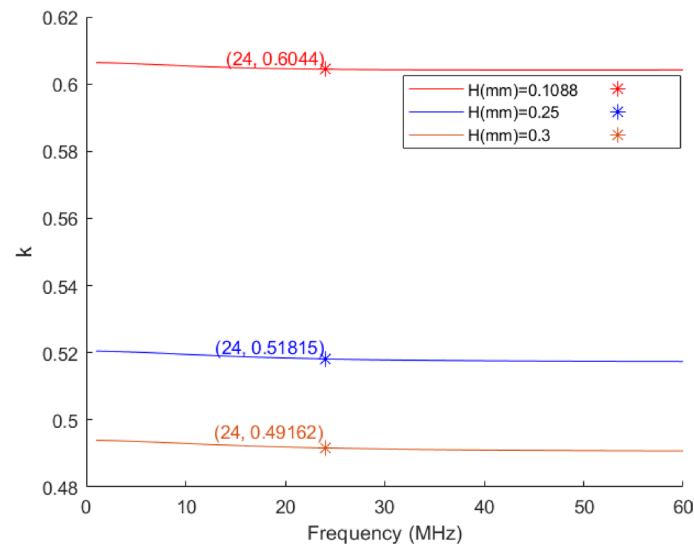**Table 1**. Coil design parameter table.

Fig. 2. Variation of the coupling coefficient k with different values of H in the frequency domain.

Planar coreless coil matching transmission and loss analysis

Wireless power transfer systems employ techniques like electromagnetic induction and magnetic resonance coupling for wireless power transmission[6]. Magnetic resonance coupling, in particular, leverages the resonance between the transmitter and receiver coils, ensuring minimal energy loss and high transfer efficiency. This study primarily investigates magnetic resonance coupling for wireless power transmission. In the practical circuit, the primary coil (T_X) of the coreless transformer is connected to a cross-coupled resonant circuit, allowing it to resonate and transfer the resonant signal to the secondary circuit through coupling with the secondary coil (R_X). In the simulation, the resonant circuit is modeled as a signal source, with the compensation capacitor C_{in} in series with the transmitter (Tx) for frequency matching with the input signal. This simulates the process of the transmitter resonating and transmitting the signal. The secondary circuit is modeled as a series combination of the load R_L and compensation capacitor C_{out}, representing the resonant signal reception by the secondary coil. To account for resistive losses in the coil wiring, the coil model simulated with Maxwell using the eddy current field and the corresponding simulation data are used. The model is subsequently imported into Simplorer, where it is integrated with the circuit, as shown in Fig. 3.
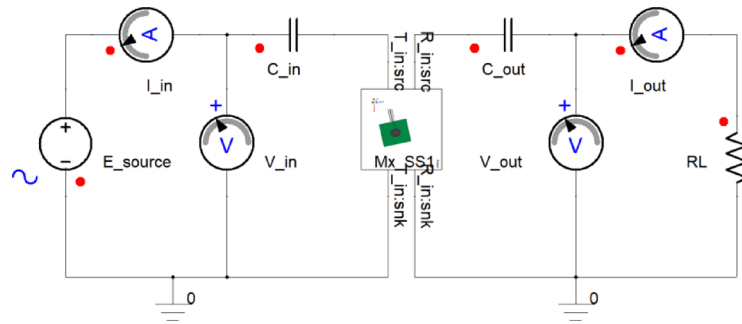
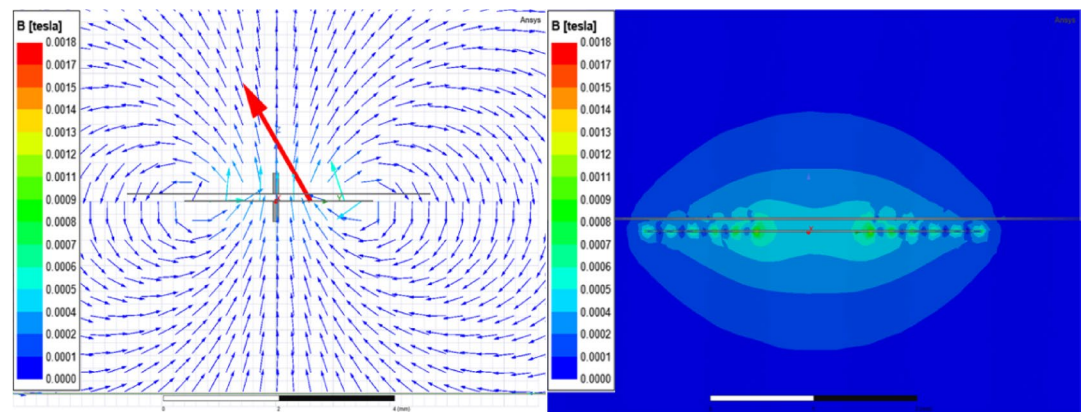**Fig. 3**. Field-circuit coupled simulation schematic.

Fig. 4. Coil magnetic flux density vector field plot and contour plot.

Here, both C_{in} and C_{out} serve the purpose of frequency matching to achieve resonant power transfer and maximize the power transmission efficiency. The capacitance C of both components is determined by the signal source frequency f_0 and the self-inductance L of the coil at that frequency:

$$f_0 = \frac{1}{2\pi\sqrt{LC}} \tag{8}$$

After conducting an eddy current simulation in Maxwell, the coil's magnetic field distribution at various operating frequencies can be analyzed. Figure 4 shows the magnetic field distribution and the corresponding contour plot of the coil at a frequency of 24 MHz.

Simplorer offers two types of simulations: Transient Analysis (TA) and AC Analysis. After performing the transient analysis, the current or voltage waveforms at the secondary output can be directly observed by representing C_{out} and R_L as a combined "load," as shown in Fig. 5. As shown in the figure, the output voltage slightly lags behind the output current, which is consistent with the simulation, where the load consists only of the capacitor C_{out} and pure resistor R_L, exhibiting a capacitive load characteristic. This validates the correctness of the combined simulation.

This study conducts AC analysis to obtain the frequency response of the circuit. In the simulation, the transmission efficiency η curve in the frequency domain is computed and plotted, and the optimal operating frequency f_0 is determined from its peak. Once the coil model parameters (W, S, L_Z, and N) are defined, and a target operating frequency of $f_0 = 24$ MHz is specified, an appropriate H value is selected. Subsequently, the eddy current field simulation is performed to extract the coil inductances L_T and L_R at f_0, from which C_{in} and C_{out} are derived using Eq. (8). This approach ensures that the transmission efficiency η achieves its maximum at the target frequency f_0 or close to it. The choice of H and R_L directly affects the transmission efficiency η. For a fixed load R_L, if H is too large, the coupling coefficient k decreases, resulting in low efficiency. Conversely, a smaller H increases k, improving efficiency.

Once H and the other coil parameters are fixed, transmission efficiency η is significantly affected by the load R_L. In practical applications, the magnitude of the load resistance R_L dictates the maximum achievable transmission efficiency. Both excessively large and small values of R_L will prevent the transmission efficiency from reaching its maximum value (aside from unavoidable losses). Moreover, since the load resistance R_L is a key impedance parameter in the circuit, an improper choice alters the circuit's impedance matching, causing the efficiency peak to shift away from the resonant frequency f_0, as shown in Fig. 6. Additionally, if the load
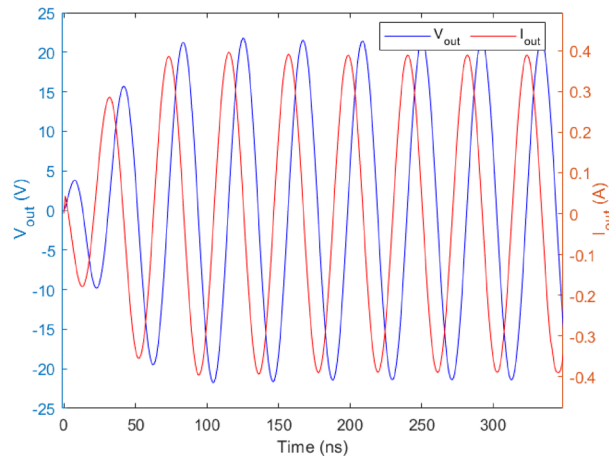
Fig. 5. Output voltage and current waveforms in transient analysis.
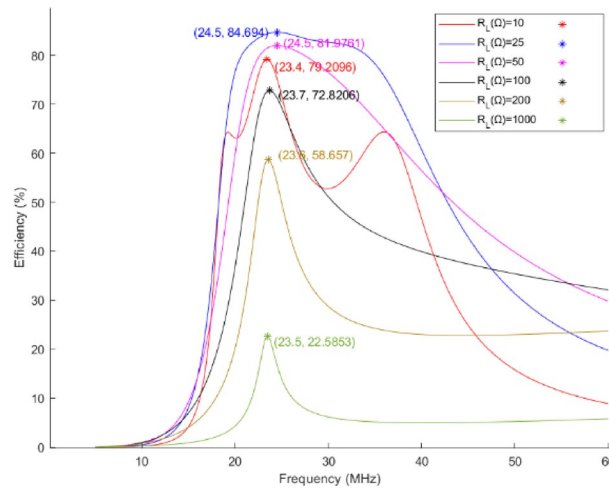

Fig. 6. Comparison of energy transfer efficiency of the coil under different load resistance conditions.

resistance is set too low, a resonant frequency splitting phenomenon may occur, causing the efficiency curve to exhibit double or multiple peaks, as shown by the $R_L=10\Omega$ curve in the figure.

During the simulation, regardless of whether H or R_L is varied, due to the intrinsic losses in the coil, the maximum transmission efficiency at the resonant frequency f_0 can never reach the ideal value. The coil losses are primarily attributed to two factors: first, the direct current resistance (DCR) of the coil, which causes the DC loss (P_{DC}) in the circuit's DC bias.

$$P_{DC} = I_{rms}{}^2 \cdot DCR$$
$$= I_{rms}{}^2 \cdot \frac{\rho \cdot \left(\sum_{i=1}^{N} \pi \cdot d_i\right)}{d_{width} \cdot d_t} \tag{9}$$

In this equation, I_{rms} is the root-mean-square (RMS) current through the coil, ρ is the resistivity of the conductor, d_i is the diameter of the i-th coil turn, d_{width} is the wire width, and d_t is the wire thickness. The second type of loss is the alternating current (AC) loss P_{AC}, which corresponds to the eddy current loss P_{eddy} in a coreless coil under high-frequency AC excitation. This loss can be computed by adding the skin effect loss P_{skin} and the proximity effect loss P_{prox}, which are orthogonal in space[7,8]. Coil winding losses can be analyzed using the Bessel function and the one-dimensional Dowell model (as shown in Fig. 7)[9–11].

The Macvicar's equations (10), upon applying the boundary conditions, reduce to (11):

$$\begin{cases} \nabla \times \nabla \times H = \nabla \times \boldsymbol{J} \\ \nabla \times E = -\mu \cdot \frac{\partial H}{\partial t} \\ \boldsymbol{J} = \sigma \cdot E \end{cases} \tag{10}$$
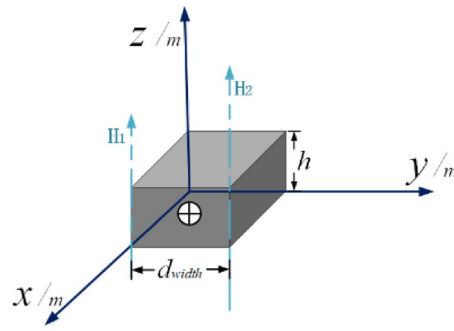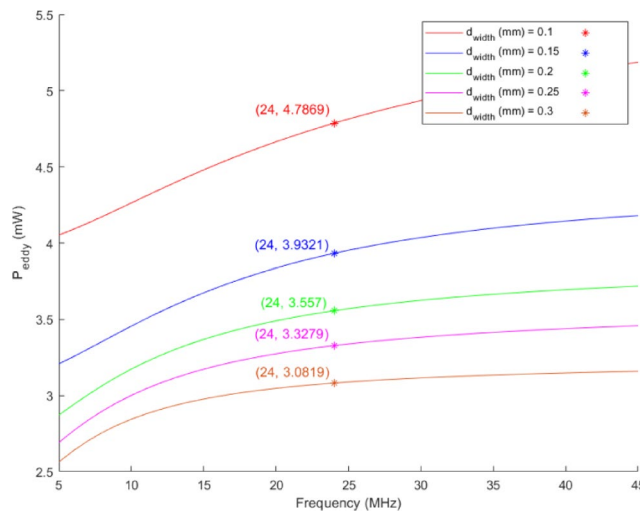
Fig. 7. One-dimensional eddy current simulation model.

Fig. 8. Variation in eddy current loss (P_{eddy}) for coils with different wire widths (d_{width}).

$$\begin{cases} \nabla^2 \mathrm{H}_{z(y)} = \mathrm{H}_{z(y)} \cdot j\omega\mu\sigma \\ \mathrm{H}_{z(y=0)} = \mathrm{H}_1 \\ \mathrm{H}_{z(y=d_{width})} = \mathrm{H}_2 \end{cases} \tag{11}$$

where $\mathbf{H}_Z$ represents the magnetic field intensity, μ is the permeability of the conductor, and σ is the resistivity of the conductor. From Eq. (11), the expression for the current density distribution $\boldsymbol{J}$ of the conductor can be further calculated, which in turn allows for the calculation of the conductor's loss per unit depth, as shown in Eq. (13).

$$\boldsymbol{J}_{x(y)} = \lambda \frac{\mathrm{H}_1 \cdot \cosh\left[\lambda \cdot (d_{width} - y)\right] - \mathrm{H}_2 \cdot \cosh\left(\lambda \cdot y\right)}{\sinh\left(\lambda \cdot d_{width}\right)} \tag{12}$$

$$P_{eddy} = \frac{h}{2 \cdot \sigma} \int_0^{d_{width}} \left| \boldsymbol{J}_{x(y)} \right|^2 dy \tag{13}$$

where $\lambda = \sqrt{\omega\mu\sigma}$. The calculation of AC losses is complex, but electromagnetic simulation software can be used for finite element analysis to estimate the AC losses in a coreless coil model. Figure 8 shows the variation of eddy current loss with different wire widths d_{width}. By determining the operating frequency f_0, the eddy current loss P_{eddy} can be approximated.

In conclusion, owing to the presence of these losses, maintaining a sufficiently high transmission efficiency requires not only the proper selection of H, R_L, and f_0, but also a comprehensive consideration of factors such as the conductor material, thickness, and trace width. Therefore, under fixed conditions of material, thickness, and trace geometry, the optimal combination of the three operating parameters—H, R_L, and f_0—should be determined to maximize the transmission efficiency and ensure high-efficiency operation of the circuit.

Optimizing algorithm design

From the preceding analysis, it is evident that the transmission efficiency of the coil is influenced by multiple variables. Considering practical design constraints, when the coil area is fixed (i.e., W, S, and N are predetermined), the transmission efficiency η is primarily governed by three key variables: the coil spacing (H), circuit load (R_L), and operating frequency (f_0). Figure 9 illustrates the smooth 3D surface plot of transmission efficiency η as a function of frequency (f) and load resistance (R_L) when $H = 0.1088$ mm and $f_0 = 24$ MHz.

As illustrated in the figure, under a fixed coil spacing H, different combinations of load resistance (R_L) and operating frequency (f) correspond to distinct transmission efficiency (η) values. To achieve the maximum possible transmission efficiency for the given coil, it is necessary to identify the optimal combination of these three variables. Following the principles of genetic algorithms (GAs), the process of selecting the optimal variable combination is essentially a parameter optimization procedure. Each combination of H, R_L, and f is treated as an individual, while the entire set of combinations constitutes the population. The transmission efficiency η serves as the fitness function for evaluating each individual. By comparing randomly generated combinations and iteratively selecting the most efficient ones, individuals undergo inheritance, mutation, and natural selection, ultimately yielding the optimal solution.

Fitness evaluation model

A parameterized eddy-current field analysis was performed in Maxwell with respect to the coil spacing parameter H. After completing this analysis, the coil model was imported into Simplorer for circuit-level co-simulation. In Simplorer, each value of H was evaluated sequentially, and a parameterized simulation was carried out with respect to the load resistance R_L. Specifically, H was assigned five representative values corresponding to typical PCB interlayer spacings. The frequency-domain analysis was conducted over the range of 5–46 MHz with a step size of 1 MHz. Meanwhile, R_L was determined through multiple comparative simulations to select twelve representative values that ensured adequate transmission efficiency. To facilitate a more comprehensive analysis of the specific coil model, it is also essential to vary the operating frequency f_0 of the signal source. In this study, f_0 was varied within the range of 5 to 45 MHz, with a step size of 1 MHz. For each simulation, the capacitance values on both sides of the circuit model were adjusted according to the self-inductance simulation results of the Maxwell coil. Subsequently, the simulation data, including f_0, H, R_L, f, and η were exported and consolidated to generate the final dataset **data**.

As established above, the transmission efficiency (η) can be regarded as a function of the operating frequency (f_0), coil spacing (H), load resistance (R_L), and signal frequency (f), which can be mathematically expressed as follows:

$$\eta = \mathrm{F}(f_0,\ H, \mathrm{R_L},\ f) \tag{14}$$

In this equation, $\mathrm{F}(f_0, H, \mathrm{R_L}, f)$ denotes an implicit functional relationship that cannot be analytically expressed. A regression model must therefore be developed to serve as a black-box predictor capable of estimating η for various combinations of (f_0, H, R_L, f). The dataset comprises approximately 84,000 samples. Employing Gaussian Process Regression (GPR) would result in a computational complexity of $O(n^3) \approx 48$ GB, which far exceeds the computational capacity of a typical workstation. In contrast, Random Forest Regression (RFR) has a lower complexity of $O(n \log n) < 1$ GB and is inherently parallelizable. Hence, the Random Forest model was thus adopted for implementation. The number of trees in the ensemble was set to 300, and simple averaging of tree predictions was used, thereby maintaining a nearly constant bias while effectively reducing model variance.

During cross-validation, the computational cost for an ensemble of 300 decision trees can be roughly estimated as $80{,}000 \times 300 \times 5$ operations. This configuration required approximately 1–2 min on a standard laptop, which is acceptable for the given dataset size. However, the computational cost increases approximately linearly with the number of folds K. As shown in Fig. 10, when K increased from 5 to 10, the average cross-
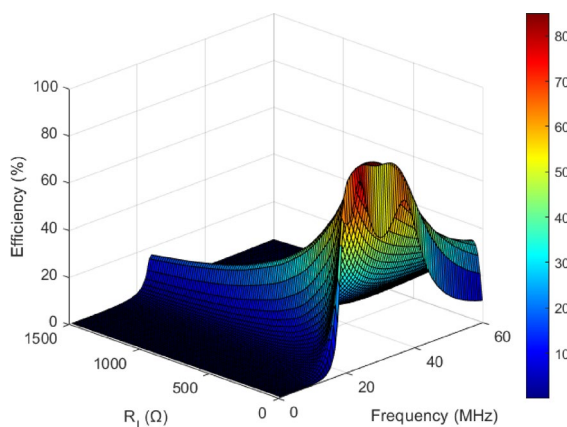

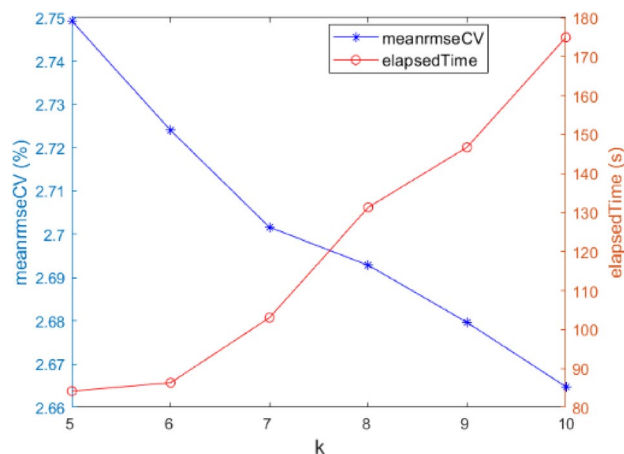**Fig. 9.** Variation of η as a function of RL and frequency (f) when $H = 0.1088$ mm.

Fig. 10. Mean error and computational time for model training with different numbers of folds (*K*).

Fig. 11. Training time and average cross-validation error of the random forest regression model.

validation error decreased slightly from 2.75% to 2.66%, while the computation time rose from 84.2 s to 174.9 s. Therefore, arbitrarily increasing *K* yields diminishing returns in accuracy relative to computational cost.

In this study, a 5-fold cross-validation was utilized to assess the model's performance. The pseudocode outlining the model training procedure is presented below.

```
cvp = cvpartition(size(X,1),'KFold',5);
for fold = 1:cvp.NumTestSets
    trainIdx = cvp.training(fold);    testIdx  = cvp.test(fold);
    Xtr = X(trainIdx,:); ytr = y(trainIdx);   Xte = X(testIdx,:);  yte = y(testIdx);
    rfMdl = fitrensemble(Xtr,ytr,'Method','Bag', 'NumLearningCycles',100,'Learners','tree');
    yhat = predict(rfMdl,Xte);
end
```

Figure 11 illustrates the average validation error and total training time of the final model trained using 5-fold cross-validation. The results show that the mean validation error is 2.745%, and the entire training process was completed within 93 s, which demonstrates satisfactory performance.

Optimization design parameters of genetic algorithm

In MATLAB, the Genetic Algorithm (GA) function can be directly called, however, it is first necessary to define the fitness function. In this study, the transmission efficiency η serves as the optimization objective, with the trained model used to predict the η value corresponding to each individual in the population. It has been observed, both in simulation and experimental validation, that η reaches its maximum when the operating frequency *f* is close to the resonant frequency f_0. This indicates the existence of a hard constraint in the optimization process, requiring that the chromosome variable *f* satisfy $|f - f_0| < 1$. This constraint must be explicitly enforced when defining the fitness function. In this study, the genetic algorithm was configured with a maximum number of generations set to 150 and a population size of 100. The iteration process was terminated early if the improvement in the best fitness value over 50 consecutive generations was less than 1×10^{-4}. To prevent premature convergence, a multi-start GA strategy was adopted, in which multiple independent runs were initialized with different random populations. After each run, the maximum efficiency η′ was compared
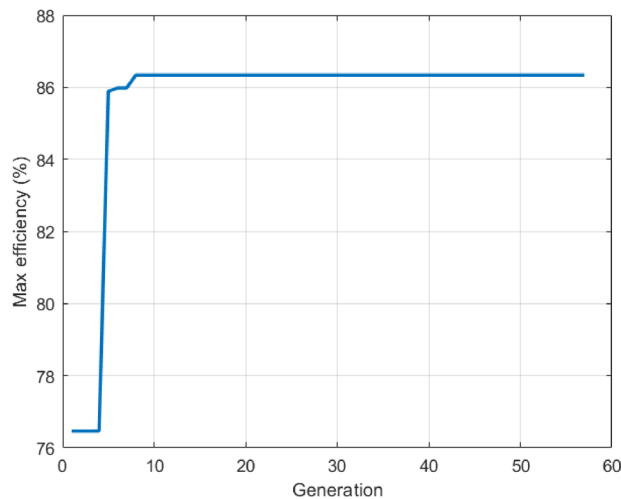
Fig. 12. Convergence behavior of the optimization algorithm throughout the entire execution process.
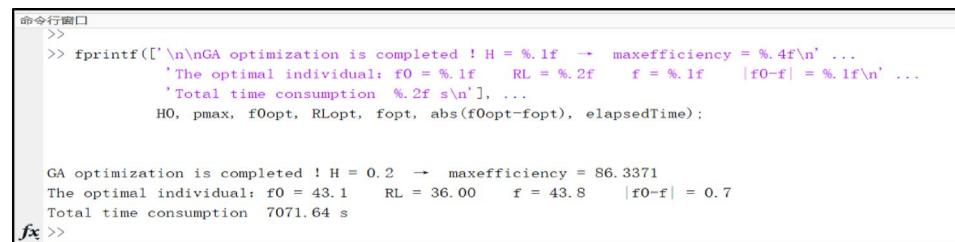

Fig. 13. Visualization of genetic algorithm optimization results and computational time.

with the current best efficiency h to determine whether to update the best individual. A total of five independent runs were performed. The pseudocode of the GA implementation is provided below:

lb = [f0min, RLmin, fmin]; ub = [f0max, RLmax, fmax];

opts = optimoptions('ga','OutputFcn',@saveBestHistory,'Display', 'off', ...

'MaxGenerations', 150,'FunctionTolerance', 1e-4,'PopulationSize', 100);

[x,fval]=ga(@fitnessGA_RF, nVar, [],[],[],[],lb,ub,[],opts); % fitnessGA_RF is a fitness function

The optimization framework implemented in this study is designed to perform parameter optimization for the coupled coil system. Given a fixed H parameter and predefined coil geometry parameters (W, S, L_Z), the algorithm searches the design parameter space (f_0, H, R_L, f) to determine the configuration that maximizes system performance. Specifically, the algorithm aims to determine the optimal parameter set (f_0, H, R_L) that yields the highest power transfer efficiency (η). During the optimization process, the η-f response was not verified to confirm whether it exhibited a single-peak characteristic under the given parameter combination (f_0, H, R_L). Consequently, frequency splitting may still occur in the coil's operation under this parameter configuration. Figure 12 shows the convergence process of the algorithm with H set to 0.2 mm. Figure 13 presents the optimal individual combination obtained after optimization, along with the total computation time. Based on the optimization results, a coupled electromagnetic simulation was conducted in Maxwell to generate the η-f curve shown in Fig. 14. Analysis of the graph shows that the efficiency (η) at 43 MHz is 88.6%, closely matching the predicted efficiency of 86.3%. The simulation results confirm the feasibility of the proposed scheme.

As shown in the figure, under this parameter combination, frequency splitting appears in the η-f curve of the coil's operation. This necessitates dynamic impedance matching in practical applications to ensure the coil operates precisely at f_0 = 43 MHz, avoiding the 'valley' between the two peaks. The algorithm can be further improved by incorporating 'unimodal' detection following the GA algorithm, such that the refresh condition for the best individual is not only that $\eta' > \eta$, but also that the η-f curve is unimodal. It is worth noting that running a single instance of the improved genetic algorithm (GA) requires at least 7 hours, even after halving parameters such as population size and convergence criteria. Adopting this enhanced algorithm would require increasing the number of independent runs, which would extend the total runtime well beyond 24 hours—resulting in a significant time overhead. Given these considerations, dynamic impedance matching is more efficiently achieved
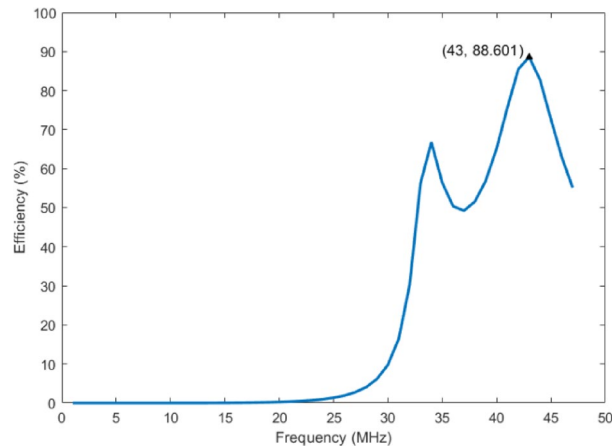
Fig. 14. η-*f* curve of the transformer based on optimization simulation results.
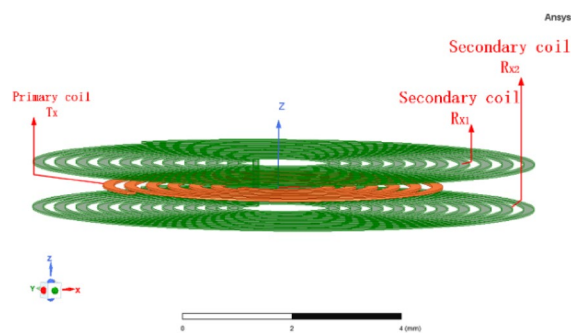

Fig. 15. Structure of the planar transformer coil.

by directly adjusting component parameters, such as the load R_L, based on the optimized results of the current algorithm. In other words, the existing optimization algorithm adequately addresses the research objectives, and further refinement of the algorithm will not be pursued here.

Application of optimization algorithms

Since the primary coil (T_X) of the coreless transformer participates in resonance within the cross-coupled resonant circuit, there is no need to consider additional capacitive compensation for the primary coil. To achieve frequency matching and enhance transmission efficiency[12], suggests using finite element analysis (FEA) software for port excitation analysis to obtain the coil model's equivalent impedance curve. This method facilitates the estimation of the coil's equivalent inductance, capacitance, and internal resistance. During this process, it is crucial to compare the static parameters of the actual coil with those of the simulated model, refine the simulation conditions, and adjust the model to better match the actual coil characteristics. This ensures accurate prediction of the coil's dynamic parameters based on port analysis results.

A Coil model is developed using the actual design parameters, and a fitness evaluation model is trained based on the parameter combinations (f_0, H, R_L, f). The trained model is then employed to predict the optimal combination for the specific H value, with selection carried out using genetic algorithm optimization. In the circuit design process, the compensation capacitor and other parameters are adjusted based on the optimization results to achieve resonant operation with maximum transmission efficiency. This approach ensures optimal coil performance under the desired operating conditions.

Sample verification

After reducing the coil's cross-sectional area (approximately 28.3 mm²), to ensure that the transformer, designed under the area constraint, achieves a certain level of transmission efficiency, a "sandwich" structure is employed for the coil. The structure comprises secondary coils on the top and bottom layers, with the primary coil in the middle, as shown in Fig. 15.

The actual sample is designed as a planar coil based on the parameters in Table 2. A corresponding model is built using electromagnetic simulation software to obtain data on different combinations and their transmission efficiencies. The data is optimized using the proposed algorithm. Figure 16 shows the comparison of transmitted and received signals of the coil before and after circuit matching, based on the optimization results. At this point, the series load (R_L) is 7 kΩ, and the parallel compensation capacitor (C_p) is 105 pF.

Parameter	Value	Parameter	Value
$H_{[N21-N1]}$ (mm)	0.21	$H_{[N22-N1]}$ (mm)	0.25
$L_{Z[N21-N1]}$ (mm)	0.0152	$L_{Z\,[N22-N1]}$ (mm)	0.035
W (mm)	0.1	S (mm)	0.1

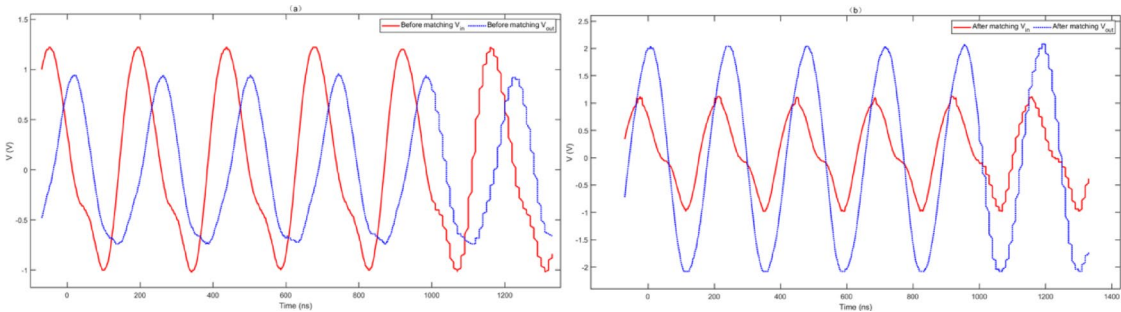**Table 2.** Sample plane coil design parameter table.

Fig. 16. Comparison of transmitted and received signal waveforms before and after matching.
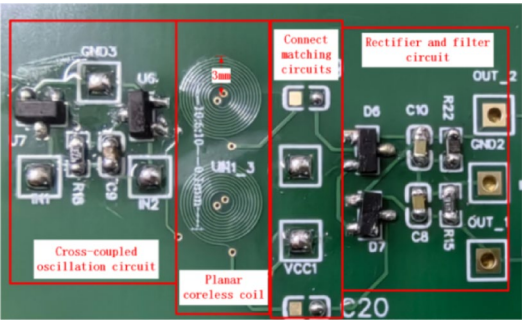

Fig. 17. Circuit diagram of the actual sample.

In the figure, (a) shows the voltage waveforms before matching, and (b) shows them after matching. The red waveform represents the primary transmitted signal, and the blue waveform represents the secondary received signal. The circuit load remains constant throughout the process. The signal transmission efficiency is approximated by comparing the peak-to-peak ratio (a) of the secondary received signal to that of the primary transmitted signal.

$$\alpha = \frac{V_{R\_PP}}{V_{T\_PP}} \tag{15}$$

The maximum value of a_{max} before matching is 0.75, and the maximum value of a_{smax} after matching is 1.62, which corresponds to an improvement of approximately 2.16 times.

Figure 17 illustrates the circuit diagram of the sample. Based on the algorithm's analysis, the matching and filter circuits are designed, and the output voltages of the secondary rectified and filtered signal before and after matching are measured, with the results shown in Table 3. A DC voltage is applied to the primary circuit of the transformer, and after resonance, the signal is magnetically coupled from the primary coil to the secondary side. By optimizing the parameters of the secondary rectifier and filter circuits for maximum efficiency, a ± 15 V control voltage is ultimately output through the push-pull circuit, after being stepped up by the converter.

In the table, V_{in} represents the peak-to-peak voltage of the input at the primary coil, V_{out} represents the peak-to-peak voltage of the output at the secondary load, and η represents the transformer energy transfer efficiency. The sample circuit testing process and its measurement results clearly show that for transformers with identical coil design parameters, the circuit can be frequency-matched to achieve the maximum transfer efficiency. However, differences in operating frequency and circuit load conditions may result in variations in the maximum transmission efficiency. According to the measurement results, when the current flowing through the load is 13.8 mA, the transformer transmission efficiency increases by 54.8% compared to the unmatched circuit. Under these conditions, the maximum transmission efficiency η_2 reaches 71.7%, which is significantly higher than the maximum efficiency achievable through frequency matching alone. In other words, although the

Parameter	$R_L = 996\Omega$		$R_L = 150\Omega$	
	Unmatched	Matched	Unmatched	Matched
V_{in} (V)	1.50	1.44	1.16	1.28
V_{out} (V)	1.78	2.48	0.87	2.07
P_{in} (mW)	80.901	42.526	47.038	56.107
P_{out} (mW)	15.713	22.979	7.956	40.233
η	19.4%	54.0%	16.9%	71.7%
Comparison	↑34.6%		↑54.8%	

Table 3. The test results of the sample circuit.

Symbol	Unit	Description	Symbol	Description
f_0	MHz	Operating signal frequency	η	Transmission efficiency
f	MHz	Actual operating frequency	k	Coupling coefficient
R_L	Ω	Circuit load	K	The fold number
H	mm	Two coil distances	T_X / R_X	Primary/secondary coil
W / d_{width}	mm	Coil width	R_{X1}	Upper secondary coil
S	mm	Coil spacing	R_{X2}	Lower secondary coil
L_Z	mm	Coil thickness	N_1	Primary coil turns
L_T / L_R	nH	Primary/secondary coil self-inductance	N_2	Secondary coil turns

Table 4. Symbol glossary.

frequency matching circuit can achieve the maximum transmission efficiency η_1 for the current load condition, the magnitude of the load also affects the transmission efficiency. If the load is improperly selected, η_1 will not equal the maximum transmission efficiency achievable by the transformer.

Conclusion
This paper presents an approach for optimizing the parameters of a planar coreless transformer using a genetic algorithm, followed by designing the transformer and circuit based on the optimization results. This study first explores the coupling characteristics of planar coreless coils, identifying the key parameters influencing transmission efficiency during energy transfer. Additionally, it analyzes the unavoidable losses inherent in the transmission process. After analyzing the factors, the paper proposes a genetic algorithm-based approach for optimizing transformer and circuit parameters. The feasibility of the proposed approach is validated through the design and testing of a sample circuit. This approach effectively reduces the time-consuming process of manually adjusting circuit components during design, improves design efficiency, and ensures the transmission circuit performance remains unchanged.

Symbol glossary
See Table 4.

Data availability
The datasets generated during and/or analysed during the current study are available from the corresponding author on reasonable request.

References
1. Dai, N., Lofti, A. W., Skutt, C., Tabisz, W. & Lee, F. C. A comparative study of high-frequency, low-profile planar transformer technologies. In *Proceedings of 1994 IEEE Applied Power Electronics Conference and Exposition - ASPEC'94. IEEE*; 226–232. (1994).
2. Xu, Q., Hu, Q., Wang, H., Mao, Z. H. & Sun, M. Optimal design of planar spiral coil for uniform magnetic field to wirelessly power Position-Free targets. *IEEE Trans. Magn.* **57** (2), 1–9 (2021).
3. Mitsuhashi, T. & Kurokawa, A. Wireless Power Transmitting Coil Achieving Uniform Magnetic Flux Density Distribution. In *2025 IEEE Radio and Wireless Symposium (RWS). IEEE*, 109–111. (2025).
4. Zhang, C., Wang, W., Xu, C. & Yang, J. Research on uniform magnetic field compensation structure of array circular coils for wireless power transfer. *IEEE Trans. Magn.* **57** (6), 1–5 (2021).
5. Lu, Y. et al. Design and implementation of LTCC coreless Transformers for intelligent solid-state switch. *Microelectron. J.* **130**, 105614 (2022).
6. Wu, N. et al. Synchronous Transmission of Power and Data for Wireless Power Transfer System Using Double LCC. In *2022 IEEE 9th International Conference on Power Electronics Systems and Applications (PESA).*, pp. 1–5. (2022).
7. Kuang, J., Ruan, X. & Ren, X. Examination of the impact of proximity and skin effects on planar magnetic element winding losses. *J. Electr. Eng. China.* **05**, 170–175 (2006).

8. Xu, C., Zhao, J. & Lin, S. Simulation study of high-frequency loss in winding of high-speed permanent magnet motor. *Agric. Equip. Veh. Eng.* **61** (02), 137–142 (2023).

9. Mao, X. & Chen, W. Modeling and analysis of AC losses in shunt PCB coils of high frequency planar Transformers for switching power supplies. *Chinese J. Electr. Eng.* **22**, 167–173 (2006).

10. Liu, B. & Chen, W. Improved high-frequency loss model for circular conductor windings with magnetic elements. *Chin. J. Electr. Eng.* **39** (09), 2795–2803 (2019).

11. Han, C. & Chen, W. Optimization of planar spiral coil for wireless power transmission. *J. Power Supply*. **18** (05), 173–179 (2020).

12. Mao, S. et al. Research on simulation method of characteristic parameters of magnetically coupled resonant wireless power transmission based on Port impedance. *Trans. China Electrotechnical Soc.* **30** (19), 95–102 (2015).

Author contributions

Wenshuang Qin：Conceptualization, Data curation, Investigation, Methodology, Software, Validation, Visualization, Writing - original draft, Writing - review & editing.Yi Zhang: Formal analysis, Supervision.Yufang Lu: Formal analysis, Funding acquisition, Methodology, Project administration, Resources.

Declarations

Competing interests

The authors declare no competing interests.

Additional information

Correspondence and requests for materials should be addressed to Y.L.

Reprints and permissions information is available at www.nature.com/reprints.

Publisher's note Springer Nature remains neutral with regard to jurisdictional claims in published maps and institutional affiliations.